Molecular Orbital Calculation and Spectroscopic Study of the Photochemical Generation of Bis(2,2′-bipyridine)rhodium(I) from Bis(2,2′-bipyridine)(oxalato)rhodium(III)

Kazuteru Shinozaki*,† and Naoto Takahashi‡

Department of Chemistry, Yokohama City University, Seto, Kanazawa-ku, Yokohama 236, Japan, and Department of Chemistry, Faculty of Science, Tokyo Institute of Technology, O-okayama, Meguro-ku, Tokyo 152, Japan

Received July 27, 1995[⊗]

A planar complex, $[Rh(bpy)_2]^+$ (bpy = 2,2′-bipyridine), was obtained from $[Rh(ox)(bpy)_2]^+$ (ox = oxalato) by photoirradiation. A rate constant k for the photoreaction was evaluated as 1×10^8 s^{-1} in simple first-order kinetics, whereas a ligand dissociation, a reorganization of the coordinated bpy, and a two-electron transfer were involved in the reaction. The process of the Rh(I) complex generation was investigated in terms of a discrete variational (DV)−Xα molecular orbital calculation on $[Rh(ox)(HN{=}CHCH{=}NH)_2]^+$ instead of $[Rh(ox)(bpy)_2]^+$. From the calculation, using the transition-state method, it was predicted that a transition of the ox π^* orbital to the metal $4d_{z^2}$ orbital caused the ligand dissociation and the reorganization of the coordinated bpy occurred in the ox π to Rh $4d_{x^2-y^2}$ excited state stabilized by the ox elimination. Upon release of the ligand and a change from octahedral to square-planar geometry, the electron density on the metal increased and the Rh 4d orbital acquired a d^8 electronic configuration.

Introduction

$[Rh(bpy)_3]^{2+}$ (bpy = 2,2′-bipyridine) and $[Rh(bpy)_2]^+$ have been investigated as intermediates in the generation of hydrogen from the photoreduction of water.[1] A series of electron-transfer reactions involving $[Rh(bpy)_2]^+$ and a hydride species were proposed in the generation of hydrogen by irradiation of a ruthenium complex in a system consisting of $[Ru(bpy)_3]^{2+}$, $RhCl_3{\cdot}3H_2O$, K_2PtCl_6, and triethanolamine (TEOA).[2] A characteristic absorption band of $[Rh(bpy)_2]^+$ was detected in the photolysis of an alkaline solution containing $[Ru(bpy)_3]^{2+}$, $[Rh(bpy)_3]^{3+}$, and TEOA.[3] Chemical reduction of $[Rh(bpy)_3]^{3+}$ with sodium borohydride or a zinc amalgam also yielded $[Rh(bpy)_2]^+$, and the Rh(I) complex was spectroscopically identified as follows.[4] A red-violet species (λ_{max} at 518 nm; $\epsilon = 9500$) was identified as $[Rh(bpy)_2(OH)_n]^{1-n}$. In neutral solution, the maximum absorbance shifted to 415 nm with a shoulder at 470 nm. In acidic solution, $[Rh(bpy)_2(H)]^{2+}$ was presumably formed as a colorless species. A violet insoluble form and a transient green form were identified as $[Rh(bpy)_2]X$ (X = Cl^-, ClO_4^-, etc.) and $[Rh(bpy)_2(H_2O)_n]^+$, respectively. In the study of the electrochemical reduction of $[Rh(bpy)_2Cl_2]^+$ and $[Rh(bpy)_3]^{3+}$, the initial electron transfer was followed by a fast elimination of bpy or Cl^-.[5] In the reaction of $[Rh(bpy)_3]^{3+}$ with $e^-(aq)$, $CO_2^{\bullet -}$, and $(CH_3)_2C^{\bullet}OH$,[4,6] a reduced species, $[Rh(bpy)_3]^{2+}$, was quantitatively and rapidly generated by the radical reductants and slowly lost bpy, and the Rh(II) complex gave the red-violet $[Rh(bpy)_2]^+$ species in a disproportionation reaction. Another Rh(II) complex was generated by photoirradiation via a reaction between $[Rh(bpy)_2]^+$ and $[Rh(bpy)_2(NO_2)_2]^+$.[7]

In the present work, the photochemistry of $[Rh(ox)(bpy)_2]^+$ (ox = oxalato) in methanol is studied. $[Rh(ox)(bpy)_2]^+$ is very photosensitive, comparable to $[Fe(ox)_3]^{3-}$ used in chemical actinometry;[8,9] the colorless Rh(III) complex is converted to a violet form by ultraviolet (UV) light irradiation. In this paper, the process involved in generation of the violet species, $[Rh^{I}(bpy)_2]^+$, from $[Rh^{III}(ox)(bpy)_2]^+$ is discussed. The violet complex is determined to be a planar structure without axial ligands and to be a two-electron-reduced species of the Rh(III) complex. A two-electron transfer, a ligand dissociation, and a reorganization of the coordinated bpy involved in the conversion from $[Rh(ox)(bpy)_2]^+$ to $[Rh(bpy)_2]^+$ are discussed in terms of a molecular orbital calculation.

Experimental Section

Materials. $[Rh(ox)(bpy)_2]ClO_4{\cdot}3H_2O$ (ox = oxalato; bpy = 2,2′-bipyridine) was prepared by a modification of a procedure for the preparation of $[Rh(ox)(en)_2]ClO_4$ (en = ethylenediamine).[10] $[Rh(bpy)_2Cl_2]Cl{\cdot}2H_2O$ (200 mg) and sodium oxalate (150 mg) were suspended in an alkaline aqueous solution (pH 9) (25 mL), and the suspension was heated to boiling for 3 min. When a freshly prepared aqueous solution (1 mL) of sodium borohydride (1 mg) was slowly added to the solution containing the Rh complex, the color of the solution turned purple. After 5 min of boiling, the purple color disappeared and a yellow solution was obtained. Activated charcoal was added to the solution. After the filtration to remove the activated charcoal, $[Rh(ox)(bpy)_2]ClO_4$ as a white-yellow precipitate was obtained by addition of 1 M perchloric acid (1 mL) to the solution. The sample was confirmed by its IR spectrum (Nujol) with CO peaks at 1665 and 1705

† Yokohama City University.
‡ Tokyo Institute of Technology.
⊗ Abstract published in *Advance ACS Abstracts,* May 15, 1996.

(1) Brown, G. M.; Chan, S.-F.; Creutz, C.; Schwarz, H. A.; Sutin, N. *J. Am. Chem. Soc.* **1979**, *101*, 7638.
(2) Lehn, J. M.; Sauvage, J. P. *Nouv. J. Chim.* **1977**, *1*, 449.
(3) Kirk, M.; Lehn, J. M.; Sauvage, J. P. *Helv. Chim. Acta* **1979**, *62*, 1345.
(4) Mulazzani, Q. G.; Emmi, S.; Hoffman, M. Z.; Venturi, M. *J. Am. Chem. Soc.* **1981**, *103*, 3362.
(5) Kew, G.; DeArmond, K.; Hanck, K. *J. Phys. Chem.* **1974**, *78*, 727.
(6) Mulazzani, Q. P.; Venturi, M.; Hoffman, M. Z. *J. Phys. Chem.* **1982**, *86*, 242.
(7) Shinozaki, K.; Yokoyama, H.; Shinohara, N. Paper presented at the Tenth International Symposium on the Photochemistry and Photophysics of Coordination Compounds, Sendai, Japan, July 1993; see Abstract P-17.
(8) Hatchard, C. G.; Parker, C. A. *Proc. R. Soc. London, Ser. A* **1956**, *235*, 518.
(9) Lee, J.; Seliger, H. H. *J. Chem. Phys.* **1964**, *40*, 519.
(10) Gillard, R. D.; Pedrosa De Jesus, J.; Sheridam, P. S. *Inorg. Synth.* **1980**, *20*, 58.

S0020-1669(95)00939-6 CCC: $12.00

cm^{-1}. Anal. Calcd for $C_{22}H_{22}N_4O_{11}ClRh$: C, 40.23; H, 3.38; N, 8.53. Found: C, 40.20; H, 3.14; N, 8.52.

Measurements. A broad band (λ > 350 nm) of a USIO 500 W Xe lamp (UXL-500D) transmitted through a Toshiba glass filter (UV-35) was used for continuous photolysis. Absorption and ^{1}H NMR spectra of samples before and after photolysis were recorded on a Shimadzu UV-2200 spectrophotometer and a JEOL FX270 FT-NMR spectrometer, respectively. A transient absorption spectrum after Xe-flash excitation (λ > 300 nm; fwhm 5 μs) was measured by a UNISOKU multichannel flash-photolysis system. An absorption rise curve of a transient species after laser excitation with a pulse width of 4−5 ns (fwhm) and a pulse-energy of 40 mJ at 266 nm (Continuum Nd:YAG Surelite I laser) was obtained on a SONY Tektronix TDS320 digital oscilloscope interfaced with an NEC PC9801 personal computer. Efficiencies for the photolyses were obtained by irradiation of the monochromatic light of a USIO 150 W Xe lamp through a monochromator for 60 s. The molarity of the Rh(I) complex was evaluated from the molar extinction coefficient (ϵ_{555nm} = 1.25 × 10^4)[11] and the absorbance at 555 nm. The fraction of the absorbed light at the irradiation wavelength[12] was normalized to that at 300 nm, which was the peak wavelength of the absorption spectrum of $[Rh(ox)(bpy)_2]^+$.

Molecular Orbital Calculation. The calculation was carried out on a SONY NEWS work station by use of a discrete variational (DV)−Xα method.[13] Model complexes $[Rh(ox)(NN)_2]^+$ and $[Rh(NN)_2]^+$, where bpy ligands were substituted by HN═CHCH═NH (NN), were calculated because bpy was too large for the calculation.[14] The geometries of the complexes were assumed on the basis of X-ray crystallographic data for $[Rh(bpy)_3]Cl_3$[15] and $[Rh(ox)_3]^{3-}$.[16,17] For $[Rh(ox)(NN)_2]^+$, ox was fixed on the *xy* plane and the two NN ligands were placed on the *yz* and *zx* planes, respectively, as shown in Figure 1. A solid arrow indicates a direction of dissociation of ox with a distance of *r*, and θ is a dihedral angle between the NN ligands. In the present calculation, distances between Rh and ox were set at r = 0, 0.5a_0, 1.0a_0, and 2.0a_0 (a_0 = 0.529 177 Å) from the position obtained from X-ray crystallography. θ values set at 0, 15, 30, and 45° represented the structural change from octahedral to square-planar. For $[Rh(NN)_2]^+$ as a planar complex, the NN ligands were placed on the *xy* plane and the *x* axis was fixed on the short axis of the ligand. Rh 1s−5p, C 1s−2p, N 1s−2p, O 1s−2p, and H 1s atomic orbitals were taken into account. Integration was taken up to 10 000 points, and a self-consistency for the orbital population within 0.001 e was obtained.

Results and Discussion

Continuous Light Irradiation. $[Rh(ox)(bpy)_2]^+$ (ox = oxalato; bpy = 2,2′-bipyridine) was sensitive to ultraviolet (UV) light, yielding a violet species in solution and in the solid state. While the violet species was considerably labile in air, it was extremely stable under anaerobic conditions. In Figure 2 is shown the UV−visible absorption spectrum of a photoproduct obtained from continuous light irradiation (λ > 350 nm) of $[Rh(ox)(bpy)_2]^+$ in N_2-saturated methanol (solid line) along with that of $[Rh(ox)(bpy)_2]^+$ (broken line). Intense absorption bands at 500−600 nm and around 300 nm were observed. The spectrum of the photoproduct was in good agreement with that of $[Rh(bpy)_2]^+$ prepared by H_2 reduction of $[Rh(bpy)_2Cl_2]^+$.[11] In the present work, $[Rh(bpy)_2]^+$ was easily prepared by UV light irradiation of $[Rh(ox)(bpy)_2]^+$ as a result of ox dissociation and reduction of Rh(III) to Rh(I). In aqueous solution, UV light irradiation yielded photoproducts different from those obtained in methanolic solution; a red-violet and a colorless species were formed in alkaline and acidic solutions, respectively. According to the literature,[4] the red-violet form, $[Rh(bpy)_2(OH)_n]^{1-n}$, in neutral or alkaline solution and the colorless one, $[Rh(bpy)_2(H)]^{2+}$, in acidic solution were presumably generated by solvent coordination, in addition to the generation of the Rh(I) species. As shown in Figure 2, the absorbance of the visible band in methanol was approximately half of that of the UV band assigned to the (π,π*) transition of bipyridine in $[Rh(ox)(bpy)_2]^+$. The visible absorption can be assigned to a charge-transfer (CT) transition because the molar extinction coefficient of $[Rh(bpy)_2]^+$ determined as 1.25 × 10^4 M^{-1} cm^{-1} [11] is as large as that of $[Fe(bpy)_3]^{2+}$ or $[Ru(bpy)_3]^{2+}$ and the absorption

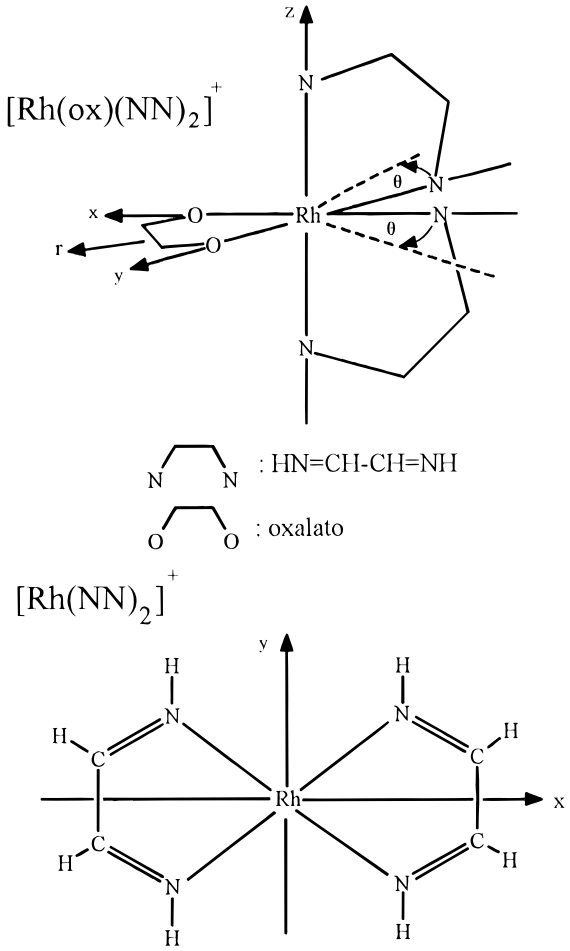

Figure 1. Molecular geometries of $[Rh(ox)(NN)_2]^+$ and $[Rh(NN)_2]^+$ (NN = HN═CHCH═NH; ox = $C_2O_4^{2-}$). The solid arrows and r represent directions of ox release and a distance, respectively, and θ is a distortion angle between the octahedral and square-planar structures.

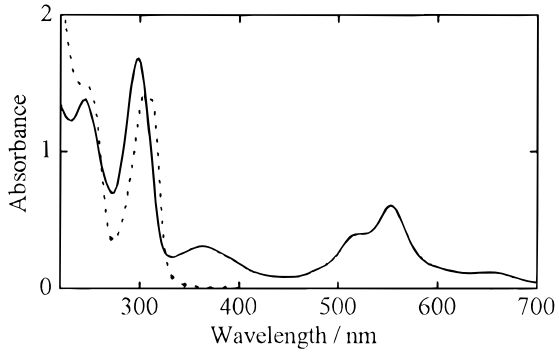

Figure 2. Absorption spectra of $[Rh(ox)(bpy)_2]^+$ (dotted line) and $[Rh(bpy)_2]^+$ (solid line) obtained from the continuous light irradiation of $[Rh(ox)(bpy)_2]^+$ in deoxygenated methanol.

(11) Chou, M.; Creutz, C.; Mahajan, D.; Sutin, N.; Zipp, A. P. *Inorg. Chem.* **1982**, *21*, 3989.
(12) Kuhn, H. J.; Braslavsky, S. E.; Schmidt, R. *Pure Appl. Chem.* **1989**, *61*, 187.
(13) Kimura, H.; Kaizu, Y.; Kobayashi, H. *Mol. Phys.* **1990**, *70*, 891 and references therein.
(14) Shinozaki, K.; Kaizu, Y. *Bull. Chem. Soc. Jpn.* **1994**, *67*, 2435.
(15) Hubesch, B.; Mahieu, B.; Meunier-Piret, J. *Bull. Soc. Chim. Belg.* **1985**, *94*, 685.
(16) Bonita, B. C.; Eriks, K. *J. Am. Chem. Soc.* **1971**, *93*, 4298.
(17) Kuroda, R. *Inorg. Chem.* **1991**, *30*, 4954.

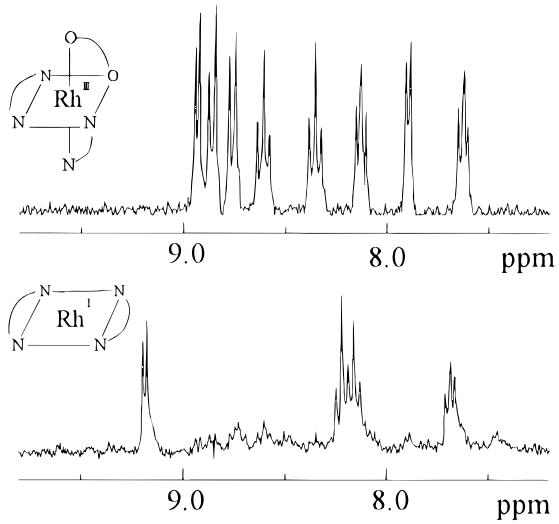

Figure 3. ^1H NMR spectra of $[Rh(ox)(bpy)_2]^+$ (top) and $[Rh(bpy)_2]^+$ (bottom) obtained by the photoirradiation in deoxygenated methanol-d_4.

maximum was shifted by the variation of solvent: $\lambda_{max} = 547$ nm in acetonitrile, $\lambda_{max} = 555$ nm in methanol, $\lambda_{max} = 558$ nm in ethanol.[18]

Eight signals were observed in the ^1H NMR spectrum of $[Rh(ox)(bpy)_2]^+$ in methanol-d_4, as shown in Figure 3. The NMR signals observed at 8−9 ppm were characteristic of metal complexes coordinated by 2,2′-bipyridine.[18−21] For the violet solution obtained by UV light irradiation, only four signals (doublet at 9.2 ppm, triplet and doublet at 8.2 ppm, triplet at 7.7 ppm) were observed and no other strong signals could be detected. The results suggest a high-symmetry molecular structure for the violet species ($[Rh(bpy)_2]^+$), and the four signals can be assigned to the 3-, 4-, 5-, and 6-protons of the pyridine ring. $[Rh(bpy)_2]^+$ is suggested to be a planar structure and to have no axial ligands in analogy to the planar structure of $[Pd(bpy)_2]^{2+}$ with the same d^8 electronic configuration as the Rh(I) complex. The photoirradiation converted $[Rh^{III}(ox)(bpy)_2]^+$ to $[Rh^{I}(bpy)_2]^+$ without byproducts and changed the geometry of the structure from octahedral to square-planar.

Pulsed Light Irradiation. Figure 4A shows the transient absorption spectrum of $[Rh(ox)(bpy)_2]^+$ obtained 5 μs after a pulse excitation. The spectrum is in very good agreement with a difference spectrum obtained by continuous light irradiation, suggesting that the conversion of Rh(III) to Rh(I) is very rapid and that $[Rh(bpy)_2]^+$ has already been generated during the excitation pulse (∼5 μs) of the Xe flash lamp. Since photoexcitation causes a one-electron transition from the ground state to the excited state, the photoinduced electron-transfer reaction is regarded as a one-electron redox process. However, two-electron reduction of Rh(III) to Rh(I) was induced by photoexcitation in this system. $[Rh(bpy)_2]^+$ was not generated in a disproportionation reaction involving Rh(II) because the absorbance of $[Rh(bpy)_2]^+$ just after the flash was proportional to that of $[Rh(ox)(bpy)_2]^+$. Although the violet color of $[Rh(bpy)_2]^+$ was immediately quenched by dissolved O_2, the absorption spectrum of $[Rh(bpy)_2]^+$ obtained just after the flash in the oxygenated solution was same as that obtained in a deoxygenated solution. This suggests that the generation of $[Rh(bpy)_2]^+$ is an intramolecular process and that its rate is faster than the rate of quenching by dissolved O_2. Considering the oxalato ion as a two-electron-reducing agent decomposed to CO_2, the following reaction mechanism can formally be given:

$$[Rh^{III}(ox)(bpy)_2]^+ + h\nu \rightarrow [Rh^{II}(CO_2^-)(bpy)_2]^+ + CO_2$$

$$[Rh^{II}(CO_2^-)(bpy)_2]^+ \rightarrow [Rh^{I}(bpy)_2]^+ + CO_2$$

The first step illustrates the photoexcitation causing the intramolecular electron transfer from ox to Rh(III) followed by the reduction of Rh(III) to Rh(II) and the decomposition of ox into CO_2 and the CO_2^- radical. The second step illustrates reactive CO_2^- reducing Rh(II) to Rh(I). An absorption change at 560 nm, which was an absorption peak of $[Rh(bpy)_2]^+$, was obtained by laser photolysis. In Figure 4B, are given the absorbance change and the excitation pulse as a dotted line and a broken line, respectively. The rise curve of absorbance after laser-pulse excitation clearly shows the generation of $[Rh(bpy)_2]^+$. The best fitting curve obtained by a deconvolution method is shown as a solid line in Figure 4B. The observed rise curve could be analyzed as a single exponential. The rate of $[Rh(bpy)_2]^+$ generation was evaluated as 1×10^8 s^{-1} from a least-squares calculation, indicating that the radical reaction and the intramolecular electron transfer, as mentioned above, are too rapid for any intermediates to be detected in our measurements. Therefore, it should be recognized that the structural change from octahedral to square-planar and the ox dissociation concurrently occurred after the photoexcitation. The reaction scheme can be presented as follows:

$$[Rh^{III}(ox)(bpy)_2]^+ + h\nu \rightarrow [Rh^{I}(bpy)_2]^+ + 2CO_2$$

Molecular Orbital Calculation. The relationship between the photoreaction and the electronic structure of the Rh complex was investigated by a molecular orbital calculation on the complex. The calculation was performed on $[Rh(ox)(NN)_2]^+$

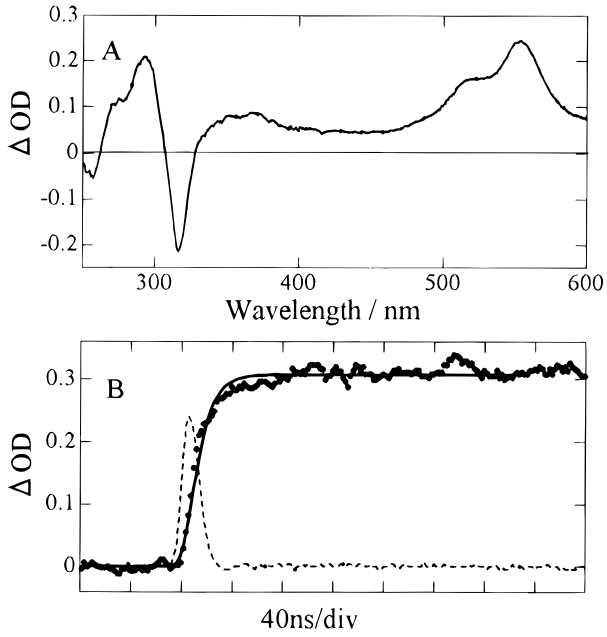

Figure 4. (A) Transient absorption spectrum of $[Rh(bpy)_2]^+$ at 5 μs after the Xe-flash pulse excitation of $[Rh(ox)(bpy)_2]^+$. (B) Absorption-rise curve (dotted line) of $[Rh(bpy)_2]^+$ monitored at 560 nm and an excitation laser pulse (broken line). The solid line is a rise curve calculated by means of a deconvolution method, and the rate constant was determined as 1×10^8 s^{-1}.

(18) Shinozaki, K.; Kaizu, Y. *Bull. Chem. Soc. Jpn.* **1994**, *67*, 2314.
(19) Constable, E. C.; Seddon, K. R. *J. Chem. Soc., Chem. Commun.* **1982**, 34.
(20) Gidney, P. M.; Gillard, R. D.; Heaton, B. T. *J. Chem. Soc., Dalton Trans.* **1972**, 2621.
(21) Lytle, F. E.; Petrosky, L. M.; Carlson, L. R. *Anal. Chim. Acta* **1971**, *57*, 239.

Table 1. Energy, Occupation Number, and Predominant Character in the Highest Occupied and the Lowest Unoccupied Molecular Orbitals in $[Rh(ox)(NN)_2]^+$ (Complex **A**) in the Ground State[a]

			predominant character/%																			
						ox						NN (HN=CHCH=NH)										
			Rh			O(1)		O(2)		C		N(*z*)		N(*xy*)		C(1)		C(2)		H(1)	H(2)	H(3)	H(4)
MO	energy/eV	occ no.	4d	5s	5p	2s	2p	2s	2p	2s	2p	2s	2p	2s	2p	2s	2p	2s	2p	1s	1s	1s	1s
⋮	⋮	⋮																					
33b	−11.764	2	11			2	51		9	2	4		3	2	10		4						1
36a	−11.577	2	43			1	6		12		4		10		11		7		5				
37a	−10.663	2	19	1	2	3	34		24		3		5		1		1		7				
34b	−9.778	2	12		1		46		35		1		2		1		1						
35b	−9.559	2	6		1	2	5		75		5		1	1	4		1		1				
38a	−9.551	2	7				42		48		1		7		14		7		14				
39a	−8.680	2	1				14		62	3	5		5		5		3		3				
36b	−8.621	0	4		1		1		2				29		29		18		15				
40a	−8.403	0	12		1		8		8		1		22		22		16		9				
41a	−6.652	0	49				11		1			9	18	2	5		1		1	2	1		
37b	−6.232	0	46			2	25		6		1				11				1				1
42a	−5.131	0	1										11		14		35		39				
38b	−5.110	0							1		1		11		14		35		38				
39b	−4.858	0			1		17		41		39						1						
43a	−1.588	0					13		25		62												
⋮	⋮	⋮																					

[a] O(1) and O(2) are the inner and outer oxygen atoms of the oxalato, respectively. N(*z*) and N(*xy*) are nitrogen atoms on the *z* axis and the *xy* plane of the NN ligands.

(**A**) (NN = HN=CHCH=NH) in C_2 symmetry by the use of a discrete variational (DV)−Xα method.[13] Main characters of the highest occupied molecular orbitals (HOMOs) and the lowest unoccupied molecular orbitals (LUMOs) of the complex are represented in Table 1. The HOMO is the 39a orbital which is separated from the other occupied orbitals in energy. The electron density in the 39a orbital is localized on the 2p orbital of the peripheral oxygen in ox. Both 36b and 40a orbitals have high electron density on nitrogen and carbon 2p orbitals in NN, and the electron densities of both 41a and 37b orbitals are rich on Rh 4d orbitals. The 39a orbital consists predominantly of an ox π orbital, and 36b and 40a are mainly NN π^* orbitals. Therefore the lowest electronic transition is the ligand-to-ligand charge-transfer (LLCT) transition. The 37b and 41a orbitals are the $4d_{x^2-y^2}$ and the $4d_{z^2}$ orbitals of the metal, respectively. The 39a → 41a and 39a → 37b electronic transitions are the ligand-to-metal charge-transfer (LMCT) transitions and are polarized to the *z* axis and the *x* (or *y*) axis, respectively. Figure 5 shows wave functions of the 39a, 36b, 40a, 41a, and 37b orbitals described as maps with contours of ±0.3, ±0.1, ±0.05, ±0.01, and ±0.005 e/a_0^3 projected onto the *xy* plane. The *x* and *y* axes (as solid arrows) and atomic positions are also shown in Figure 5. The Rh−O bonds and the C−C bond of ox in the 36b and 40a orbitals are shown to have bonding character. However 37b and 41a show antibonding character in both the Rh−O bonds and the C−C bond. From the wavefunction maps, it is predicted that photoexcitation of 39a → 37b and/or 39a → 41a causes ox dissociation and decomposition of ox into the CO_2^- radical or CO_2 but that photoexcitation of 39a → 36b and 39a → 40a cannot eliminate the ox ligand.

The lowest oxalato-to-rhodium charge-transfer (LMCT) states and the lowest NN (π,π^*) states in $[Rh(ox)(NN)_2]^+$ were calculated. Figure 6 shows the transition energies and the oscillator strengths (*f*) obtained by the transition-state method.[22−26]

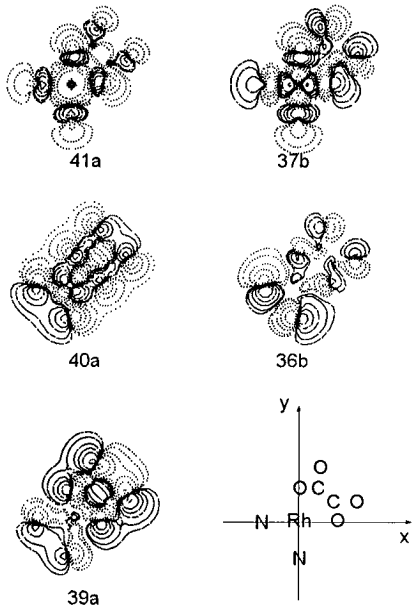

Figure 5. Contour maps projected onto the *xy* plane of the 39a, 36b, 40a, 41a, and 37b orbitals in $[Rh(ox)(NN)_2]^+$ (**A**). The positive (solid) and negative (dotted) contours are drawn at ±0.3, ±0.1, ±0.05, ±0.01, and ±0.005 e/a_0^3, respectively.

The energies of the LMCT excitations (39a → 41a and 39a → 37b) were calculated as 21.0×10^3 and 23.4×10^3 cm^{-1}, respectively, and the oscillator strengths were evaluated as $f = 0.0003$ and 0.0046, respectively. The other LMCT excitations with large oscillator strengths were predicted in the UV region; for example, the 35b → 37b transition was calculated as that with $f = 0.1176$ at 30.1×10^3 cm^{-1}. It is shown that the lowest LMCT excitations of 39a → 41a and 39a → 37b have considerably low intensities. The (π,π^*) transitions of the diimine ligands were calculated as symmetry-allowed transitions with large oscillator strengths around 30×10^3 and 37×10^3 cm^{-1}. It has been reported that the oscillator strength of the (π,π^*) excitations of a bpy complex was larger than that of an imine (RCH=NCH_3) complex; UV bands were mainly simu-

(22) Slater, J. C. In *Advances in Quantum Chemistry*; Lowdin, P. O., Ed.; Academic Press: New York, 1972; Vol. 6, p 1.
(23) Slater, J. C. *Quantum Theory of Molecules and Solids*; McGraw-Hill: New York, 1974; Vol. 4.
(24) Slater, J. C. *Phys. Rev.* **1951**, *81*, 385.
(25) Slater, J. C.; Wilson, T. M.; Wood, J. H. *Phys. Rev.* **1969**, *179*, 28.
(26) Johnson, K. H.; Smith, F. C. *Phys. Rev. B* **1972**, *5*, 831.

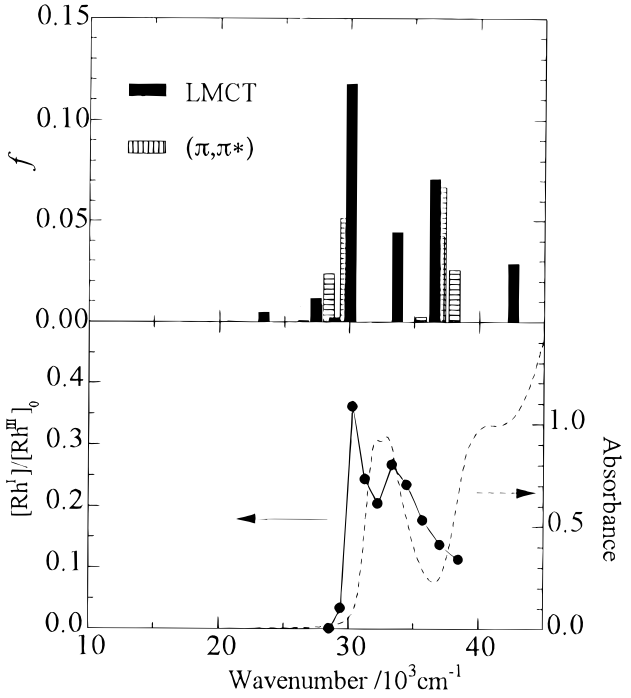

Figure 6. Top: Energy levels and oscillator strengths (*f*) of the oxalato-to-metal charge-transfer (LMCT) transitions and the (π,π*) transitions of $[Rh(ox)(NN)_2]^+$. Bottom: Molar ratios ($[Rh^I]/[Rh^{III}]_0$) in the photolysis as a function of excitation wavelength and an absorption spectrum (broken line) of $[Rh(ox)(bpy)_2]^+$. $[Rh^I]$ and $[Rh^{III}]_0$ are the molarities of $[Rh(bpy)_2]^+$ and $[Rh(ox)(bpy)_2]^+$, respectively.

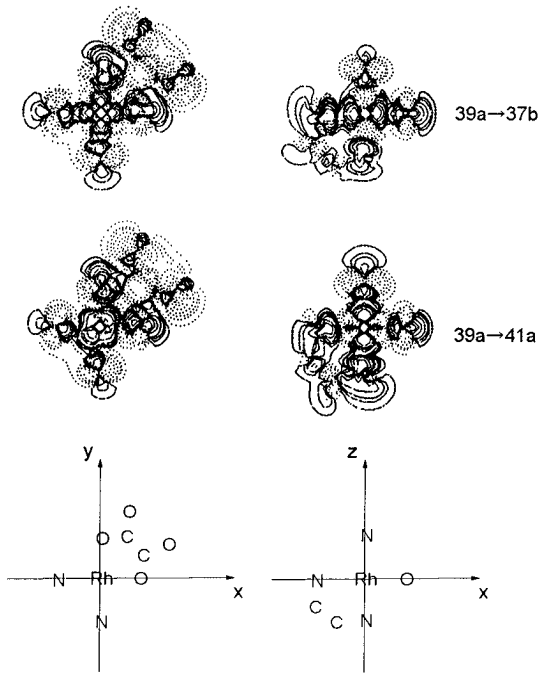

Figure 7. Electron density maps drawn as difference contours between the excited state and the ground state. The maps projected onto the *xy* plane and the *zx* plane present the variation of the total electron density induced by the oxalato-to-metal charge-transfer transitions 39a → 37b ($4d_{x^2-y^2}$) (upper) and 39a → 41a (d_{z^2}) (lower). The solid and dotted contours represent the increased and decreased populations, respectively, and are given at ±0.0001, ±0.0003, ±0.0005, ±0.001, ±0.0025, ±0.005, ±0.01, and ±0.02 e/a_0^3, respectively.

lated as the (π,π*) transitions of coordinated bpy.[27] In the present calculation, it seems that the calculated (π,π*) transitions correspond to the twin bands of $[Rh(ox)(bpy)_2]^+$ at 33×10^3 and 40×10^3 cm^{-1} as a broken line. The ratios of the concentration of the photogenerated $[Rh(bpy)_2]^+$ ($[Rh^I]$) and the initial concentration of $[Rh(ox)(bpy)_2]^+$ ($[Rh^{III}]_0$) are shown in Figure 6 as a function of the excitation wavelength. The absorption band inducing the efficient photodecomposition is given by the maximum of $[Rh^I]/[Rh^{III}]_0$ at 30.0×10^3 cm^{-1} (330 nm). It is suggested that the (π,π*) band is not the most photolabile band. In the present calculation, it is predicted that the LMCT bands will be in the low-energy region of the (π,π*) bands. The spectrum of $[Rh^I]/[Rh^{III}]_0$ reveals that the photoreaction efficiently occurs in the LMCT excited state. The LMCT transitions are divided into A and B representations in C_2 symmetry. The lowest LMCT transitions (39a → 37b and 39a → 41a) occur in A and B, respectively. The electron migration following the LMCT transitions in A and B is clarified by the difference in electron densities between the ground and the excited state.

Figure 7 shows difference maps of the total electron density between the ground state and the LMCT excited state (39a → 37b and 39a → 41a) of $[Rh(ox)(NN)_2]^+$. The solid contour represents the increase of the electron density in the LMCT excited state from that in the ground state, and the dotted one shows the decrease of the electron density. The LMCT excitation to the 37b (Rh $4d_{x^2-y^2}$) orbital gives rise to increases in the electron densities of the nitrogen atoms in NN and the oxygen atoms in ox in the xy plane and to a decrease in the σ electron density of the nitrogen atoms in NN on the z axis. Therefore the photoexcitation to the 37b orbital strengthens the Rh−O bonds instead of weakening them. In contrast, the excitation 39a(ox π) → 41a(Rh $4d_{z^2}$) decreases the σ electron density of the nitrogen and oxygen atoms in the *xy* plane. The difference in π electron density of the nitrogen and oxygen atoms in the 39a → 41a excited state is same as that in the 39a → 37b excited state. The contour maps reveal that the 39a → 41a photoexcitation weakens the Rh−O and Rh−N bonds in the *xy* plane and induces ox dissociation.

To clarify the ox elimination after photoexcitation, three complexes different in geometry were calculated in addition to the calculation on $[Rh(ox)(NN)_2]^+$ (**A**). Each ox in the complexes was kept away from the central metal along the direction of the arrow in the *xy* plane as shown in Figure 1. They were set at distances of $r = 0.5a_0$ (**B**), a_0 (**C**), and $2a_0$ (**D**), respectively, from the position given by the X-ray crystallographic data. The two NN ligands were fixed on the *yz* and *zx* planes, respectively, and all of the complexes (**A**−**D**) were assumed to have C_2 symmetry. The ox dissociation process was represented by the four geometries in the order **A**, **B**, **C**, and **D**. Energy diagrams for the complexes obtained from the calculation are shown in Figure 8. The energies of the 41a and 37b orbitals are dramatically lowered upon release of ox, while those of the 39a, 36b, and 40a orbitals are independent of the Rh−ox distances. It is presumed that not only the 41a orbital but also the 37b orbital play important roles in the ox dissociation. While the energy of the 41a orbital is lower than that of the 37b orbital at $r = 0$ (**A**), the energy of the 37b orbital is lower than that of the 41a orbital at $r \geq 0.5a_0$ (**B**, **C**, **D**). The 37b orbital is more stabilized in the energy than the 41a orbital in the ox dissociation process. Wave functions of the 39a, 36b, 40a, 37b, and 41a orbitals of **D** are shown in Figure 9. The antibonding characters of the C−C bond of ox in the 37b and 41a orbitals are slightly enhanced in the ox elimination. In both the 37b and 41a orbitals, the direction of the lobes of the π orbital of the nitrogen atoms in NN of **D** are markedly inclined

(27) Maruyama, M.; Matsuzawa, H.; Kaizu, Y. *Inorg. Chem.* **1995**, *34*, 3232.

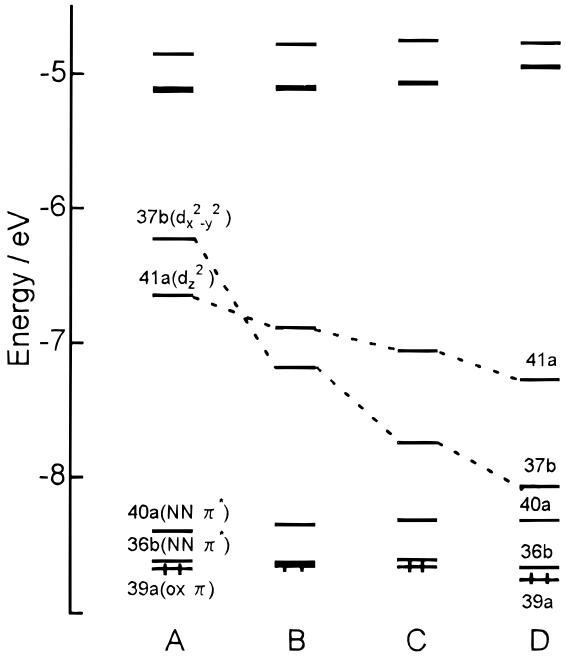

Figure 8. Variation of the energy levels of the highest occupied and the lowest unoccupied molecular orbitals of $[Rh(ox)(NN)_2]^+$ in the ox dissociation process. The distances between Rh and ox are extended as $0.5a_0$ (**B**), $1.0a_0$ (**C**), and $2.0a_0$ (**D**) compared with that in **A**. See text.

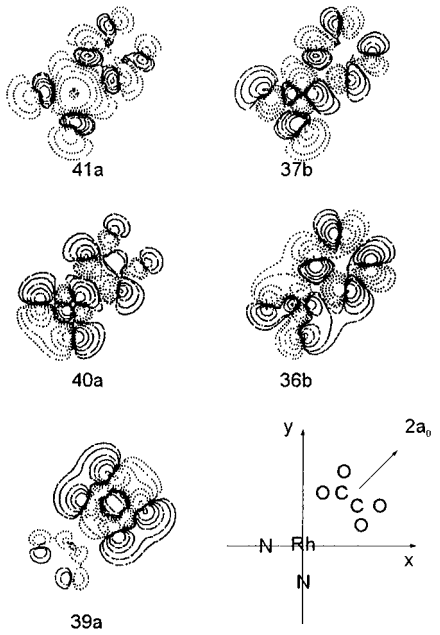

Figure 9. Contour maps projected onto the *xy* plane of the 39a, 36b, 40a, 41a, and 37b orbitals in complex **D**. The positive (solid) and negative (dotted) contours are drawn at ±0.3, ±0.1, ±0.05, ±0.01, and ±0.005 e/a_0^3, respectively.

compared with that of **A**. Since the lobes of the nitrogen atoms in the 37b orbital of **D** are mutually shown as having antibonding character, the electronic interaction between the nitrogen atoms is suggested to be more repulsive than that in **A**. In contrast, that in the 41a orbital is attractive because of bonding character between the nitrogen atoms. Wave functions of the other nitrogen atoms set on the *z* axis in the 37b orbital are almost the same in **A** and **D**. It is predicted that the repulsive force between the nitrogen atoms in the 39a → 37b excited state causes the reorganization of bpy in the Rh(III) complex after the dissociation of ox. Figure 10 shows the energy level diagrams of HOMOs and LUMOs of complexes **A** and **B** in the conformational change from octahedral to square-planar. Variations of the energy levels in the conformational conversion processes before and after the ox elimination are illustrated in the left and right sides of Figure 10, respectively. The reorganization of coordinated bpy is represented in the order $\theta = 0$, 5, 15, and 30°; the structure of the complex with $\theta = 0°$ is the octahedral; and the complex with $\theta = 45°$ consists of the square-planar $[Rh(ox)(NN)_2]^+$ moiety and ox. In both the diagrams, the 37b orbital stabilizes in energy with increasing distortion angle θ, though the 41a orbital is unstable in the distorted structure with $\theta = 30°$ compared with the octahedral structure ($\theta = 0°$). The energy of the 41a orbital of **B** (with $r = 0.5a_0$) at 30° is remarkably higher than that of **A** (with $r = 0$) at 30°. The crossing of the energy levels of the 41a and 37b orbitals between 15 and 30° for complex **A** is also observed in the case of ox dissociation. Energies of the 40a and 36b orbitals as NN π* orbitals increase with increasing distortion angle, and the 39a orbital energy also slightly depends on the angle. The stabilization of the 37b orbital is suggested to be important in the bpy-reorganization process. It is concluded that ox elimination and reorganization of bpy occur in the 39a → 37b state because of the switch to the lowest LMCT excited state from the 39a → 37b to the 39a → 41a state after the extension of the Rh−ox bond length due to the photoexcitation of 39a → 41a.

The number of electrons on the Rh 4d orbitals of $[Rh(ox)(NN)_2]^+$ in the ground state is 7.65, larger than the value of 6.00 expected from the d^6 electronic configuration of Rh(III) because of the σ donation of oxygen and nitrogen atoms in ox and NN. In the LMCT excited states, this number is increased by 0.07 (39a → 37b) and 0.08 (39a → 41a) from that in the ground state. The LMCT excitations of 39a → 37b and 39a → 41a induce an increase in the total number of electrons on the metal by 0.14 (39a → 37b) and 0.15 (39a → 41a) and a decrease in that on ox by 0.06 (39a → 37b) and 0.12 (39a → 41a). The electron populations on the metal are varied in the ox-elimination and the bpy-reorganization processes. The number of 4d electrons increases with extension of the distance between Rh and ox, e.g. 7.65 (**A**, $r = 0$), 7.66 (**B**, $r = 0.5a_0$), 7.68 (**C**, $r = 1.0a_0$), and 7.74 (**D**, $r = 2.0a_0$). The numbers of total electrons on the metal in the complexes are nearly the same at 44.34 (**A**), 44.31 (**B**), 44.32 (**C**), and 44.35 (**D**) because of the electron migration in the complexes. Electronic structures were also calculated on the complexes with $r = 0$ and various dihedral angles such as $\theta = 5$, 15, and 30°, where the θ values represent the octahedral−planar structural change as shown in Figure 1. From the calculation, the numbers of 4d electrons were obtained as 7.64 ($\theta = 5°$), 7.62 ($\theta = 15°$), and 7.64 ($\theta = 30°$) and were independent of the dihedral angle θ, while the total electrons on the metal increased as 44.34 ($\theta = 5°$), 44.35 ($\theta = 15°$), 44.45 ($\theta = 30°$). It seems that the electron migration is inhibited by the distortion from the octahedral to the planar structure and that the electron density on the metal is richest in a planar-Rh-$(NN)_2$ moiety. From the calculations on $[Rh(NN)_2]^+$ (**E**) of the final photoproduct and $[Rh(ox)(NN)_2]^+$ with $r = 10a_0$ and $\theta = 45°$ (**F**), which has the planar-Rh$(NN)_2$ moiety, the numbers of 4d electrons were evaluated to be 7.98 and 8.00, respectively. They are in good agreement with that expected from the d^8 electronic configuration of Rh(I). The surplus two electrons on ox ($C_2O_4^{2-}$) are completely transferred to the planar-Rh-$(NN)_2$ moiety in complex **F**. The number of the electrons on ox is same as the value of 44.00 for a neutral molecule C_2O_4 which is presumed to be unstable. Table 2 lists HOMOs and LUMOs with their predominant characters of **E**(D_{2h}) and **F**(C_2). The 37a, 39a, 36b, and 38b orbitals in **F** are completely localized

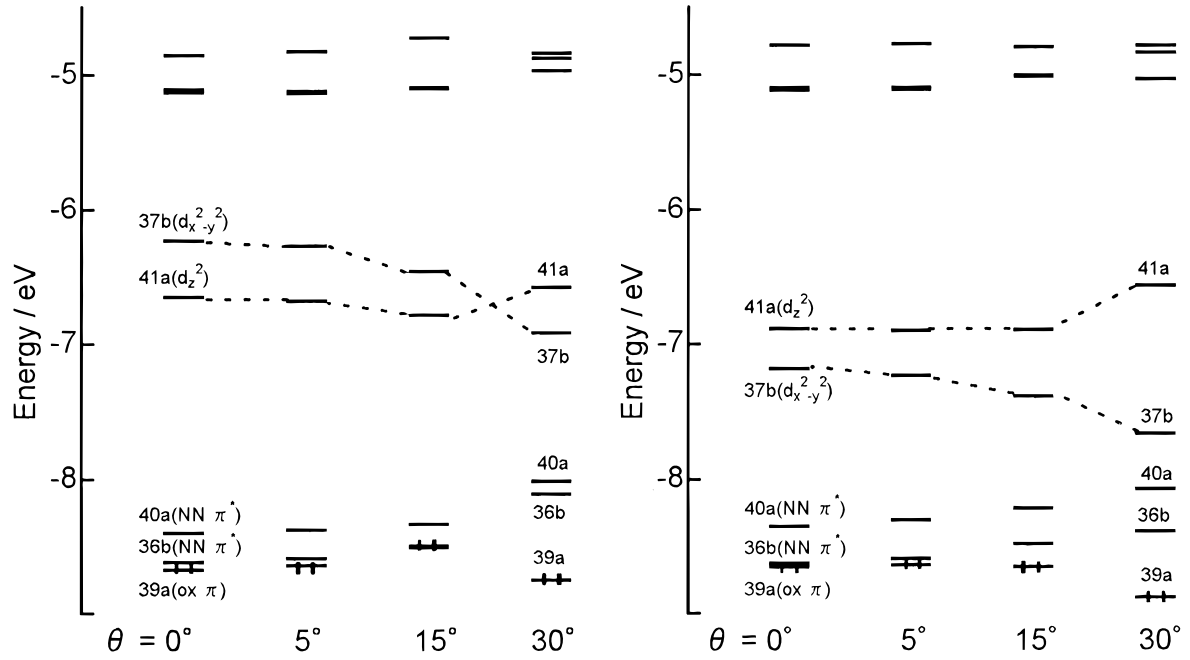

Figure 10. Variation of the energy levels of the highest occupied and the lowest unoccupied molecular orbitals of complexes **A** (left) and **B** (right) in the distortion from the octahedral to the square-planar structure. The distortion angles are set at 0, 5, 15, and 30°, respectively.

Table 2. Energy, Occupation Number, and Predominant Character in the Highest Occupied and the Lowest Unoccupied Molecular Orbitals in $[Rh(ox)(NN)_2]^+$ with $\theta = 45°$ and $r = 10a_0$ (Complex **F**) and $[Rh(NN)_2]^+$ (Complex **E**) in the Ground State[a]

$[Rh(ox)(NN)_2]^+$ (**F**) in C_2 Symmetry

			predominant character/%														
						ox						NN (HN═CHCH═NH)					
			Rh			O(1)		O(2)		C(ox)		N(NN)		C(NN)		H(1)	H(2)
MO	energy/eV	occ no.	4d	5s	5p	2s	2p	2s	2p	2s	2p	2s	2p	2s	2p	1s	1s
36a	−9.691	2	95												2	1	1
37a	−9.577	2					57		43								
35b	−9.077	2	78										7		14		
38a	−9.019	2	79	17									4				
39a	−8.954	2					32		58	3	7						
36b	−8.832	0					58		42								
40a	−8.400	0			9								51		40		
37b	−6.952	0	26										53		20		
38b	−4.925	0					26		32		42						
41a	−4.748	0	57									12	23		6	1	1
42a	−4.390	0	2										26		71		
39b	−4.226	0	4										28		68		

$[Rh(NN)_2]^+$ (**E**) in D_{2h} Symmetry

			predominant character/%								
						NN (HN═CHCH═NH)					
			Rh			N		C		H(1)	H(2)
MO	energy/eV	occ no.	4d	5s	5p	2s	2p	2s	2p	1s	1s
$14a_g$	−9.508	2	94	1				1	2	2	
$3b_{2g}$	−9.186	2	78				8		14		
$15a_g$	−8.943	2	79	17		1	3				
$5b_{1u}$	−8.576	0			9		50		41		
$4b_{2g}$	−7.133	0	29				52		20		
$8b_{1g}$	−4.750	0	59			12	23		3		1
$2a_u$	−4.501	0					25		75		
$4b_{3g}$	−4.331	0	4				27		70		

[a] O(1) and O(2) are the inner and outer oxygen atoms of the oxalato ligand, respectively.

on ox, while the others are localized on the $Rh(NN)_2$ moiety. The electronic structure of the $Rh(NN)_2$ moiety in **F** is much the same as that of **E**; for example, 38a and 37b orbitals in **F** correspond to $15a_g$ and $4b_{2g}$ orbitals in **E**, respectively.

In complex **E**, the highest occupied orbitals, $15a_g$ (d_{z^2}) and $3b_{2g}$ (d_{zx}), are localized on the Rh 4d orbitals, and the lowest unoccupied orbitals, $5b_{1u}$ and $4b_{2g}$, consist of NN π^* orbitals. The lowest transitions such as $15a_g \rightarrow 5b_{1u}$, $15a_g \rightarrow 4b_{2g}$, $3b_{2g} \rightarrow 5b_{1u}$, and $3b_{2g} \rightarrow 4b_{2g}$ are metal-to-ligand charge-transfer (MLCT) transitions. This supports the assignment of the visible absorption band of $[Rh(bpy)_2]^+$ expected from the spectroscopic results. The allowed $15a_g \rightarrow 5b_{1u}$ ($d_{z^2} \rightarrow \pi^*$) and $3b_{2g} \rightarrow 5b_{1u}$

($d_{zx} \rightarrow \pi^*$) transitions are polarized to the *z* and *x* axes, respectively, where the *z* axis is perpendicular to the molecular plane and the *x* axis is the short axis of the ligand.

Concluding Remarks

Some oxalato (ox) complexes ($[Fe(ox)_3]^{3-}$ and UO_2ox) can be utilized to evaluate quantum yields in chemical actinometry,[8,9,28] though the reaction mechanism is complicated without a simple stoichiometry. UV or near-UV light irradiation of $[Fe(ox)_3]^{3-}$ forms an Fe^{2+} ion with quantum yields ($\Phi = 1.01-1.25$) which are independent of light intensity, with decomposition of ox into CO_2, CO, HCO_2H, etc. The reaction scheme is presented as follows:

$$[Fe(C_2O_4)_n]^{(3-2n)+} + h\nu \rightarrow Fe^{2+} + (n-1)C_2O_4^{2-} + C_2O_4^{-}$$

$$[Fe(C_2O_4)_n]^{(3-2n)+} + C_2O_4^{-} \rightarrow Fe^{2+} + nC_2O_4^{2-} + 2CO_2$$

In the case of the photolysis of $[Rh(ox)(bpy)_2]^+$, ox, which decomposed into CO_2, was a two-electron donor and Rh(III) accepted the electrons in the intramolecular process. The photoreactive excited state was neither metal centered nor ligand centered but was a ligand-to-metal charge-transfer excited state. This was supported by a molecular orbital calculation and measurements of the photochemical quantum yields as a function of the irradiation wavelength. We concluded that the elimination of ox and the reorganization of the coordinated bpy occurred concurrently in this system, and the $[Rh(bpy)_2]^+$ generation process involving the drastic structural change was analyzed in first-order kinetics. Therefore the reation mechanism could be analyzed by a molecular orbital calculation based on a Walsh diagram.[29,30] In the present calculation, the triplet states of the complexes were not taken into account. However, the excited-state energy obtained by the transition-state method is interpreted as the mean energy of the excited singlet and the triplet.[13] The energy stabilization of the 37b and 41a orbitals in the structural change is that of the ^{1,3}(39a $\rightarrow$ 41a) and ^{1,3}(39a $\rightarrow$ 37b) states.

Acknowledgment. We thank Prof. N. Shinohara, Yokohama City University, for measurements of the transient absorption spectra and helpful discussions.

IC950939Z

(28) Leighton, W. G.; Forbes, G. S. *J. Am. Chem. Soc.* **1930**, *52*, 3139.
(29) Walsh, A. D. *J. Chem. Soc.* **1953**, 2260.
(30) Buenker, R. J.; Peyerimhoff, S. D. *Chem. Rev.* **1974**, *74*, 127.